

AMUSE-VIRGO. II: DOWN-SIZING IN BLACK HOLE ACCRETION

ELENA GALLO^{1,2}, TOMMASO TREU^{3,4}, PHILIP J. MARSHALL^{5,6}, JONG-HAK WOO⁷,
CHRISTIAN LEIPSKI⁸, & ROBERT ANTONUCCI³

Draft version December 3, 2021

ABSTRACT

We complete the census of nuclear X-ray activity in 100 early type Virgo galaxies observed by the *Chandra X-ray Telescope* as part of the AMUSE-Virgo survey, down to a (3σ) limiting luminosity of 3.7×10^{38} erg s⁻¹ over 0.5-7 keV. The stellar mass distribution of the targeted sample, which is mostly composed of formally ‘inactive’ galaxies, peaks below $10^{10} M_{\odot}$, a regime where the very existence of nuclear super-massive black holes (SMBHs) is debated. Out of 100 objects, 32 show a nuclear X-ray source, including 6 hybrid nuclei which also host a massive nuclear cluster as visible from archival *Hubble Space Telescope* images. After carefully accounting for contamination from nuclear low-mass X-ray binaries based on the shape and normalization of their X-ray luminosity function, we conclude that between 24–34% of the galaxies in our sample host a X-ray active SMBH (at the 95% C.L.). This sets a firm lower limit to the black hole occupation fraction in nearby bulges within a cluster environment. The differential logarithmic X-ray luminosity function of active SMBHs scales with the X-ray luminosity as $L_X^{-0.4 \pm 0.1}$ up to 10^{42} erg s⁻¹. At face value, the active fraction –down to our luminosity limit– is found to increase with host stellar mass. However, taking into account selection effects, we find that the average Eddington-scaled X-ray luminosity scales with black hole mass as $M_{\text{BH}}^{-0.62^{+0.13}_{-0.12}}$, with an intrinsic scatter of $0.46^{+0.08}_{-0.06}$ dex. This finding can be interpreted as observational evidence for ‘down-sizing’ of black hole accretion in local early types, that is, low mass black holes shine relatively closer to their Eddington limit than higher mass objects. As a consequence, the fraction of active galaxies, defined as those above a fixed X-ray Eddington ratio, *decreases* with increasing black hole mass.

Subject headings: black hole physics – galaxies: clusters: individual (Virgo)

1. INTRODUCTION

Historically speaking, active galaxies are characterized by compact nuclei with abnormally high luminosity and fast variability ascribed to accretion of mass onto a super-massive black hole (SMBH). While the term AGN (active galactic nuclei) generally refers to nuclear luminosities in excess of 10^{43-44} erg s⁻¹, the distinction between active and inactive is rather arbitrary, that is, is set by our ability to detect and interpret signatures of accretion-powered activity. From elaboration of the Soltan argument (Soltan 1982) follows that, since black holes have grown mostly via radiatively efficient accretion as powerful quasars (e.g. Yu & Tremaine 2002; Marconi et al. 2004; Merloni & Heinz 2008; Shankar, Weinberg & Miralda-Escudé 2009), nearby galaxies ought to harbor, if anything, only weakly accreting black holes. The alleged ubiquity of SMBHs at the center of (massive) galaxies, together with the realization that BHs play a crucial role in regulating the assembly history and evolution of their hosts (Kormendy & Richstone 1995; Kormendy et al. 1997; Magorrian et al. 1998; Gebhardt et al. 2000; Ferrarese & Merritt 2000; McLure & Dunlop 2002; Marconi & Hunt 2003; Ferrarese

& Ford 2005; Gültekin et al. 2009), have spurred a series of searches for active nuclei in the nearby universe at different wavelengths, each with its own advantages and limitations. In particular, the low mass end of the black hole mass function in the local universe (Greene & Ho 2007, 2009) remains poorly constrained, and can only be explored indirectly, as even the highest angular resolution attainable with current instrumentation is not sufficient to go after a $\lesssim 10^6 M_{\odot}$ black hole through resolved stellar kinematics, except for exceptionally nearby systems. (see Bentz et al. 2009 on nearby, reverberation-mapped AGN).

Amongst the general population of galaxies, optical studies suggest that nuclear activity is quite common (43% of all galaxies in the Palomar sample; Ho, Filippenko & Sargent 1997; Ho 2008). The percentage raises substantially in galaxies with a prominent bulge component, approaching 70% for Hubble types E-Sb. The dependence of the nuclear properties on Hubble type – with late type objects displaying active fractions as low as 10% – has been confirmed by numerous other studies (e.g. Kauffmann et al. 2003; Miller et al. 2003; Decarli et al. 2007), although a recent work based on high-resolution mid-infrared spectrometry of a sample of (32) inactive galaxies, suggests that the AGN detection rate in late-type galaxies is possibly 4 times larger than what optical observations alone indicate (Satyapal et al. 2008). Since the enormous wealth of data from the Sloan Digital Sky Survey (SDSS) became available, various environmental effects on nuclear activity have been investigated, such as host galaxy properties (Kauffmann et al. 2003, 2004; Rich et al. 2005; Kewley et al. 2006; Schawinski et al. 2007, 2009; Kauffmann, Heckman & Best 2008) local density and large scale environment (Kauffmann et al. 2003, 2004; Constantin & Vogeley 2006; Constantin et al. 2008; Choi et al. 2009).

¹ MIT Kavli Institute for Astrophysics and Space Research, 70 Vassar St., Cambridge, MA 02139

² Hubble Fellow

³ Physics Department, University of California Santa Barbara, CA 93106

⁴ Packard Fellow

⁵ Kavli Institute for Particle Astrophysics and Cosmology, Menlo Park, CA 94025

⁶ Kavli Fellow

⁷ Astronomy Program, Department of Physics and Astronomy, Seoul National University, Seoul, Korea

⁸ Max Planck Institute for Astronomy, Königstuhl 17, D-69117 Heidelberg, Germany

While AGN were first discovered as powerful, unresolved optical sources at the center of galaxies, emission at higher frequencies, hard X-rays and gamma-rays, is almost univocally associated with non thermal processes related to accretion, such as Comptonization of thermal photons in a hot electron-positron plasma. Hard X-rays in particular offer a clean-cut diagnostics, and a relatively unexplored one, to pinpoint low accretion power SMBHs in nearby galaxies. So far, searches for nuclear X-ray sources in formally inactive galaxies have been somewhat sparse and focused on the high-mass end of the local population. Prior to the launch of *Chandra* and *XMM-Newton*, such observations were effectively limited to X-ray luminosities $\gtrsim 10^{40}$ erg s⁻¹ even in the nearest elliptical galaxies (e.g.: Canizares, Fabbiano & Trinchieri 1987; Fabbiano et al. 1993; Fabbiano & Juda 1997; Allen, Di Matteo & Fabian 2000). Due to the lack of sensitivity and angular resolution, earlier mission were necessarily deemed to confusion between accretion-powered sources of various nature, most notably nuclear vs. off-nuclear, and also thermally emitting gas. As an example, Roberts & Warwick (2000), report on the detection of 54 X-ray cores out of 83 Palomar galaxies targeted by *ROSAT*. As also noted by Ho (2008), a significant (dominant, we argue) fraction of the cores' X-ray flux may be due to unresolved emission from X-ray binaries. The greatly improved sensitivity and angular resolution of *Chandra* and *XMM-Newton* have made it possible to investigate nuclear emission associated with SMBHs orders of magnitude deeper, effectively bridging the gap between AGN and inactive galaxies (e.g. Di Matteo et al. 2000, 2001, 2003; Ho et al. 2001; Loewenstein et al. 2001; Sarazin, Irwin & Bregman 2001; Fabbiano et al. 2003, 2004; Terashima & Wilson 2003; Pellegrini 2005; Soria et al. 2006a, 2006b; Santra et al. 2007; Pellegrini, Ciotti & Ostriker 2007; Ghosh et al. 2008; Zhang et al. 2009).

Direct measurements of bolometric Eddington ratios in *bona fide* AGN are typically no lower than 10^{-3} (e.g. Woo & Urry 2002; Kollmeier et al. 2006; Heckman et al. 2004). As a comparison, the inferred Eddington-scaled X-ray luminosities of inactive galaxies – that is, of their nuclear SMBHs – are as low as 10^{-8} : in those massive elliptical galaxies where the temperature and density profiles of the thermally-emitting gas can be reconstructed and used to estimate the inner gas reservoir available to accretion, the measured nuclear X-ray luminosities are orders of magnitude lower than expected from Bondi-type accretion onto the nuclear SMBH (e.g. Pellegrini 2005; Soria et al. 2006a,b). However, most X-ray studies target massive nearby elliptical galaxies, and are thus biased towards the high mass end of the SMBH mass function. In order to expand our knowledge about black hole demographics in the local universe, it is necessary to explore both the low mass and the low-luminosity end of the distribution.

Even in the nearby universe, pushing the threshold down to X-ray luminosities as low as a few 10^{38} erg s⁻¹ necessarily means facing contamination from bright X-ray binaries within the instrument point spread function (PSF). This problem has been touched upon in a recent work by Zhang et al. (2009), who collected archival *Chandra* observations of 187 galaxies (both late and early types) within 15 Mpc. 86 of them host nuclear X-ray cores, the majority of which, based on the fitted slope of their differential luminosity function, are attributed to low-level accretion onto SMBHs, rather than to X-ray binaries. The issue of X-ray binary contamination becomes particularly delicate when the inferred X-ray active

fractions are then used to place constraints on the local black hole occupation fraction. From an observational standpoint, the very existence of SMBHs in nearby dwarf galaxies remains a matter of investigation. Ferrarese et al. (2006a) argue that the creation of a 'central massive object', be it a black hole or a compact stellar nucleus, would be the natural byproduct of galaxy evolution, with the former being more common in massive bright galaxies (with absolute B magnitude M_B brighter than -20), and the latter dominating –possibly taking over– at magnitudes fainter than -18 (see also Wehner & Harris 2006, and Kormendy et al. 2009). Massive nuclear star clusters (e.g. Seth et al. 2008, 2010; Graham & Spitler 2009), with inferred radii around a few tens of pc, become increasingly prominent down the mass function. When dealing with faint X-ray cores ($10^{38} - 10^{39}$ erg s⁻¹), the problem of X-ray binary contamination is further exacerbated by the presence of a nuclear star cluster, having higher stellar encounter rates, and hence a higher X-ray binary fraction with respect to the field. In order to deliver an unbiased census of nuclear activity for nearby galaxies down to X-ray luminosities as low as the Eddington limit for a solar mass object, not only it is mandatory to deal with nearby sources, but it also becomes necessary to have information about their stellar content within the X-ray instrument PSF, specifically the presence/absence of a nuclear star cluster. Additionally, in order to avoid contamination from the short lived, X-ray bright, high-mass X-ray binaries, deep X-ray searches for weakly active SMBHs (down to $\sim 10^{38}$ erg s⁻¹) should be preferentially limited to the nuclei of early type galaxies.

To this purpose, and with these caveats in mind, in Cycle 8 we proposed and were awarded a large *Chandra/Spitzer* program to observe 100 (84 new+16 archival) spheroidal galaxies in the Virgo Cluster (AMUSE-Virgo: PI: Treu, 454 ks). The targeted sample is that of the *Hubble* Virgo Cluster Survey (VCS; Côté et al. 2004). For each galaxy, the high resolution *g* and *z* band images enable us to resolve, when present, the nuclear star cluster, infer its enclosed mass (following Ferrarese et al. 2006a; see Ferrarese et al. 2006b, for a detailed isophotal analysis of the *Hubble* data), and thus estimate the chance contamination from a low-mass X-ray binary (LMXB) as bright/brighter than the detected X-ray core based on the shape and normalization of the LMXB luminosity function in external galaxies (see §3, and references therein).

As a part of the AMUSE-Virgo survey, each VCS galaxy was observed with *Chandra* for a minimum of 5.4 ks, which, at the average distance of Virgo (16.5 Mpc; Mei et al. 2007; see also Blakeslee et al. 2009), yields a (3σ) sensitivity threshold of 3.75×10^{38} erg s⁻¹ over the *Chandra* bandpass. The *Chandra* results from the first 32 targets (16 new + 16, typical more massive, archival observations) have been presented by Gallo et al. (2008; hereafter Paper I.). Point-like X-ray emission from a position coincident with the optical nucleus was detected in 50 per cent of the galaxies. We argued that, for this sub-sample, all of the detected nuclear X-ray sources are most likely powered by low-level accretion on to a SMBH, with a $\lesssim 11$ per cent chance contamination from LMXBs in one case only (VCC1178=NGC 4486B, for which independent evidence points towards the presence of a nuclear BH; Lauer et al. 1996). The incidence of nuclear X-ray activity increases with the stellar mass M_* of the host galaxy: only between 3–44% of the galaxies with $M_* < 10^{10} M_\odot$ harbor an

X-ray active SMBH. The fraction rises to between 49–87% in galaxies with stellar mass above $10^{10} M_{\odot}$. (at the 95% C.L.).

In Paper II, we complete the X-ray analysis of the whole AMUSE-Virgo sample: the final deliverable product of this study is an unbiased census of accretion-powered luminosity in a galaxy cluster environment, and thus the first measurement of the SMBH activity duty cycle. The Paper is organized as follows: § 2 summarizes our analysis of the new *Chandra* data and the stacking procedure. In § 3 we carefully address the issue of contamination from low-mass X-ray binaries to the detected X-ray cores. § 4 and 5 presents our main results, specifically on the active fraction, dependence of accretion luminosity on black hole mass and X-ray luminosity function. We discuss the implications of our results in § 6, and conclude with summary in § 7. We refer the reader to Paper I for a thorough description of the program, as well as the determination of the parameters (such as stellar masses, stellar velocity dispersions, and black hole masses) employed throughout this series. In a companion paper, we report on the results from the *Spitzer* 24 μm observations of the same sample (Leipski et al., Paper III.).

2. DATA ANALYSIS

A detailed description of the *Chandra* data analysis, and the cross-correlation to HST images is given in Paper I., § 3. Here we summarize only the most relevant steps. We observed each galaxy with the Advanced CCD Imaging Spectrometer (ACIS) detector for 5.4 ks of nominal exposure time in Faint-mode. The target was placed at the aim point of the back-side illuminated S3 chip. Standard level 2 event lists, processed for cosmic ray rejection and good time filtering, were employed. We first checked for background flares and removed time intervals with background rate $\gtrsim 3\sigma$ above the mean level. Further analysis was restricted to energies between 0.3–7.0 keV in order to avoid calibration uncertainties at low energies and to limit background contaminations at high energies. We applied a wavelet detection algorithm over each activated chip, using CIAO *wavdetect* with sensitivity threshold corresponding to a 10^{-6} chance of detecting one spurious source per PSF element if the local background is uniformly distributed. The *Chandra* astrometry was improved by cross-matching the detected (non-nuclear) X-ray sources with the SDSS catalog (Data Release 5, DR5), and the resulting bore-sight corrections were applied to the data following the method described by Zhao et al. (2005). Individual source locations are subject to statistical uncertainties affecting the centroiding algorithm and to the dispersion of photons due to the PSF. For ACIS-S, Garmire et al. (2000) estimate 90 per cent confidences of $\pm 0''.5$ for sources with ~ 10 counts, $\pm 0''.2$ for 20–50 count sources, and negligible for >100 count sources. The statistical uncertainties affecting the centroid errors in the positions of the X-ray sources, combined with the $\lesssim 0''.1$ positional error of SDSS, results in a final astrometric frame that is accurate to between $0''.2$ (fields with $\gtrsim 20$ counts sources) and $0''.5$ (fields with faint sources). After registering the *Chandra* images to SDSS, we ran again *wavdetect* to refine the positions, and searched for point-like X-ray emission centered at the galaxy optical center, derived from archival *Hubble* ACS images registered to the SDSS world coordinate system as described in Paper I, § 3.3. We searched for X-ray counterparts to the optical nuclei within an error circle which is the quadratic sum of the positional uncertainty for the X-ray source, the uncertainty in the optical astrometry, and the uncertainty in the X-ray bore-

sight correction, multiplied by the chosen confidence level scale factor (3σ). All the newly detected X-ray nuclei are consistent with being point-like based on a comparison with the normalized point spread functions. A circular region with a $2''$ radius centered on X-ray centroid position, and an annulus with inner radius $20''$ and outer radius $30''$ were adopted for extracting the nuclear X-ray counts and for background subtraction, respectively. Given the low number statistics we are typically dealing with, we estimated the corresponding fluxes using *webPimms*⁹, and assuming an absorbed power-law model with photon index $\Gamma = 2$ and hydrogen equivalent column $N_{\text{H}} = 2.5 \times 10^{20} \text{ cm}^{-2}$ (the nominal Galactic value determined from the HI studies of Dickey & Lockman 1990). While the adopted photon index is relatively steep compared to the indices generally quoted in the literature for active nuclei ($1.4 \lesssim \Gamma \lesssim 1.7$), this value is more representative of the low luminosity population ($1.6 \lesssim \Gamma \lesssim 2$; e.g. Terashima & Wilson 2003). In particular, we obtained $\Gamma = 2 \pm 0.2$ by stacking the detected X-ray nuclei in our sample and fitting their cumulative spectrum, as discussed in § 3.1.

Under the above-mentioned assumptions, $10^{-3} \text{ count s}^{-1}$ in the 0.3–7 keV energy band correspond to an intrinsic flux of $3.5 \times 10^{-15} \text{ erg cm}^{-2} \text{ s}^{-1}$ between 2–10 keV (ACIS-S). In case of no significant detection we applied Poisson statistics to derive upper limits on the nuclear luminosity at the 95 per cent confidence level (Gehrels 1986). Table 1. summarizes our results; 32/100 galaxies are found to host a X-ray core. While 51/100 show a massive nuclear star cluster (see Table 3 in Ferrarese et al. 2006b, for the fitted g and z magnitudes and half light radii), only 6 out of the 32 X-ray cores are classified as hybrid, i.e. hosting both a X-ray nucleus and a star cluster.

3. LOW-MASS X-RAY BINARY CONTAMINATION

In a broad stellar mass range, and in the absence of a nuclear star cluster, the total number of LMXBs and their cumulative X-ray luminosity are proportional to the stellar mass of the host galaxy, M_{\star} (Gilfanov 2004; Kim & Fabbiano 2004; Humphrey & Buote 2004). The number n_{X} of expected sources per unit stellar mass above a certain luminosity threshold can be estimated from the X-ray luminosity function for LMXBs (the functional expression given by Gilfanov 2004 is employed throughout this series). In turn, the number of expected sources within the *Chandra* PSF (convolved with the positional uncertainty) is given by n_{X} times $M_{\star, \text{PSF}}$: the stellar mass within the central aperture. As detailed in Paper I, the number of expected LMXBs above the X-ray luminosity threshold of AMUSE-Virgo is typically lower than a few 10^{-2} at an average distance of 16.5 Mpc. Given the functional expression of the LMXB luminosity function¹⁰, it can also be ruled out that any nuclear X-ray source be due to a collection of fainter LMXBs, as the integral $\int dn/dL_{\text{X}} \cdot dL_{\text{X}}$ is dominated by the luminosity term.

As discussed in the introduction, the very existence of SMBHs in faint inactive galaxies remains questionable. In fact, Ferrarese et al. (2006a) suggest that compact stellar nuclei tend to be more common than nuclear SMBHs at the low-mass/low-luminosity end of the galaxy mass function, possi-

⁹ <http://heasarc.gsfc.nasa.gov/Tools/w3pimms.html>

¹⁰ Following Gilfanov (2004), the differential X-ray luminosity function of LMXBs in early types is parametrized as a power law with two breaks: dn/dL_{X} scales as $L_{\text{X}}^{-\alpha}$, where $\alpha = 1.0$ between $5 \times 10^{35} - 2 \times 10^{37} \text{ erg s}^{-1}$, $\alpha = 1.9$ between $2 \times 10^{37} - 5 \times 10^{38} \text{ erg s}^{-1}$, and $\alpha = 4.8$ above $5 \times 10^{38} \text{ erg s}^{-1}$.

bly taking over at magnitudes fainter than -18 (this does not necessarily implies that nuclear SMBHs and star clusters can not possibly coexist; see e.g. Seth et al. 2008; Graham & Spitler 2009). For the purpose of this work, the presence of a nuclear star cluster, having an enhanced stellar encounter rate, implies a higher chance contamination from LMXBs with respect to the nuclei of massive early type galaxies, which, on the contrary, show a light deficiency with respect to standard Sersic profiles (Ferrarese et al. 2006a; Côté et al. 2006, 2007; Kormendy et al. 2009). In order to account for this effect, in the presence of a nucleated galaxy we conservatively adopt the X-ray luminosity function of LMXBs in *globular clusters*, as estimated by Sivakoff et al. (2007). It is known that, while hosting a small percentage of the galaxy stellar mass, globular clusters are home to about 50% (with an admittedly large scatter) of the observed LMXBs. In this environment, the number of expected LMXB sources scales non-linearly with the cluster mass. Sivakoff et al. (2007) derive an expression for the expected number¹¹ n_X of LMXBs brighter than 3.2×10^{38} erg s^{-1} (the luminosity limit is set by the sample completeness) in a star cluster of stellar mass M_* , half mass radius r_h (incidentally, this is about the same completeness limit of our Virgo sample).

For our faint, nucleated spheroidals, the mass of the nuclear star cluster can be estimated from Equation 1 in Ferrarese et al. (2006a), using the colors and half-light radii given in Table 3 by Ferrarese et al. (2006b). The expected number of LMXBs in a globular cluster can then be converted to a probability P_X that there is at least one LMXB brighter than the detected X-ray luminosity assuming a Poisson distribution. In terms of chance probability of hosting a X-ray active SMBH, each of the 6 galaxies which host both a nuclear X-ray sources and a massive star cluster is then assigned a weight $(1 - P_X)$: see Table 2. for details¹². This yields our final, *weighted* distribution of galaxies hosting a active (down to our luminosity threshold) SMBH.

3.1. Stacking Analysis

In order to place more stringent limits on the average flux, we stacked the 0.3-7 keV images of the 64 non-detected nuclei with snapshot observations¹³, for a total of 328 ks of effective exposure. We extracted the counts from a $2''$ radius circular aperture, and background from an annulus with inner and outer radii $R_{in}=25''$ and $R_{out}=30''$, centered on the stacked nuclear position (see Figure 1, left panel). 49 counts are detected within the $2''$ radius aperture, while 12.8 are expected from the background, indicating a statistically significant detection (null detection probability lower than 2×10^{-7}). At a

$$^{11} n_X \propto 8 \times 10^{-2} (M_*/10^6 M_\odot)^{1.237} (r_h/1 \text{ pc})^{-2.22}$$

¹² As discussed in Paper I, the optical radial profile of VCC1178 also shows marginal evidence for a nuclear star cluster. We estimate the probability of hosting a LMXB within the *Chandra* PSF to be $\sim 12\%$, hence $w = 1 - P_X = 0.88$. However, we assigned $w = 1$ to the nuclear X-ray source in VCC1178 based on independent evidence that this galaxy hosts a nuclear SMBH, specifically the presence of a double optical nucleus (see Lauer et al. 1996).

¹³ For the stacking analysis, we only used those galaxies with snapshot, 5.4 ks observations, for a total of 64 targets. The remaining 4 galaxies with non-detections are: VCC1226, VCC0881, VCC798 and VCC1535. Being massive ellipticals with deep archival exposures, all four galaxies have substantial contamination to the soft X-ray band from diffuse gas emission, which is the main reason why we did not include them in the stacking analysis. In these 4 cases, the search for nuclear X-ray sources was performed in the hard X-ray band only, as described in detail in § 3.2 of Paper I.

distance of 16.5 Mpc, and assuming an absorbed power law model as discussed in the previous section, the measured net count rate ($1.0 \pm 0.2 \times 10^{-4}$ count s^{-1}) corresponds to an *average*, unabsorbed 0.3-7 keV luminosity $\langle L_X \rangle = 3.5 \pm 0.7 \times 10^{37}$ erg s^{-1} . This emission can be accounted for by an ensemble of low-luminosity LMXBs within the total stellar mass enclosed by the *Chandra* PSFs: following Gilfanov (2004), the expected X-ray luminosity due to LMXBs within all of the 64 nuclei (enclosing about $10^{10} M_\odot$) is $6 \pm 2 \times 10^{37}$ erg s^{-1} . In terms of average Eddington scaled luminosity, this sets an upper limit of 3×10^{-8} for an average nuclear black hole mass $\langle M_{BH} \rangle = 10^{6.9} M_\odot$.

We also grouped the 64 observations into two sets of 32 observations corresponding to two black hole mass bins, with $\langle M_{BH} \rangle_a = 10^{8.0} M_\odot$ and $\langle M_{BH} \rangle_b = 10^{6.4} M_\odot$, and stacked them into 2 observations by 164 ks. Both show a statistically significant nuclear detection: the measured net count rates for observations *a* and *b* are $1.3 \pm 0.3 \times 10^{-4}$ count s^{-1} , and $0.7 \pm 0.2 \times 10^{-4}$ count s^{-1} . Again, the inferred luminosities are consistent with what expected from faint nuclear LMXBs. They translate into the following Eddington-scaled luminosities: $\langle L_X/L_{Edd} \rangle_a < 3.0 \times 10^{-9}$ and $\langle L_X/L_{Edd} \rangle_b < 6.4 \times 10^{-8}$, respectively. The middle and right panels of Figure 1 show the two stacked images with 32 galaxies each: low- M_{BH} bin and high- M_{BH} bin, respectively.

Finally, in order to characterize the average spectral properties of our sample, we stacked the images of all the detected X-ray nuclei with snapshot observations, for a total of 102 ks of effective exposure; 236 ± 16 counts are detected from stacked nuclear X-ray source, corresponding to a net count rate of $2.3 \pm 0.1 \times 10^{-3}$ count s^{-1} (0.3-7 keV). We constructed the soft (S), medium (M) and hard (H) band stacked images, restricting the energies between 0.3-0.7 keV, 0.7-1.1 keV, and 1.1-6 keV, respectively (e.g. Ott, Walter & Brinks 2005). The net counts in each band (S= 30.1 ± 5.9 , M= 73.1 ± 8.8 , and H= 130.8 ± 8.0) yield the following hardness ratios for the stacked nucleus: $HR1 = (S-M-H)/(S+M+H) = -0.7 \pm 0.1$, and $HR2 = (S+M-H)/(S+M+H) = -0.1 \pm 0.1$. These relatively hard values of HR1 and HR2 are quite typical of accretion powered sources, such as AGN or X-ray binaries, confirming our interpretation of low-level accretion-powered emission (rather than thermal emission from hot gas, as observed e.g. in star forming regions).

4. THE DUTY CYCLE OF NUCLEAR ACTIVITY

4.1. The active fraction vs. host stellar mass

The *weighted* (as described in § 3) distribution of galaxies hosting a X-ray active SMBH down to our luminosity limit is plotted in Figure 2 as a function of the host stellar mass M_* . Overall, we infer that between 24–34% of the galaxies targeted by AMUSE-Virgo host a X-ray active SMBH, down to a luminosity threshold of $\sim 2 \times 10^{38}$ erg s^{-1} (2-10 keV, at the 95% C.L.). *This sets a firm lower limit to the black hole occupation fraction in nearby bulges within a cluster environment.*

Perhaps not surprisingly, the incidence of nuclear activity increases with stellar mass: between 0.7–14% of the galaxies with $\log(M_*)$ between 8.5–9.5 host a nuclear, active SMBH; the fraction raises to 16–43% for $9.5 < \log(M_*) < 10.5$, up to 53–87% for $\log(M_*) > 10.5$ (at the 95% confidence level). The known trend (since the first Palomar sample; Ho et al. 1997) of increasing active SMBH fraction with increasing host stellar mass is obviously amplified by (possibly entirely

driven by) the fact that, going down the mass function, as the nuclear BH masses decrease with (some power of) M_* , so do their expected X-ray luminosities for a fixed Eddington ratio.

In order to assess this completeness effect, we estimated the fraction of X-ray active SMBHs as a function of M_* for four sub-samples, each complete down to $L_X/L_{\text{Edd}} = -9, -8, -7, -6$. These ‘Eddington-complete’ active fractions are listed in Table 3 as a function of M_* : within the limitations of the admittedly large error bars imposed by such low statistics sub-samples, this exercise proves that *once the issue of Eddington completeness is taken into account, there is no evidence for a statistically significant increase in the incidence of nuclear SMBH activity with increasing host stellar mass*. For reference, Figure 3 illustrates the distribution of the inferred Eddington scaled X-ray luminosities for the AMUSE-Virgo sample as a function of M_{BH} (in red), and compares it with previous works (Pellegrini et al. 2005; Soria et al. 2006a,b; Zhang et al. 2009). While the distribution of active SMBHs is quite broad in terms of Eddington-scaled X-ray luminosities, with L_{Edd} ranging between a few 10^{-9} up to a few 10^{-6} , this plot seems to show a slight increase of the Eddington-scaled X-ray luminosity with black hole mass. We quantify this in the following section.

4.2. Accretion luminosity vs. black hole mass

We have chosen to focus on the Eddington-scaled X-ray luminosity as the more physically meaningful quantity; to investigate more rigorously the connection between accretion-powered X-ray luminosity and black hole mass, in this section we infer the parameters of a power law relationship between the measured L_X and M_{BH} through a Bayesian approach:

$$\log(\hat{L}_X/10^{38} \text{ erg s}^{-1}) = A + B \log(\hat{M}_{\text{BH}}/10^8 M_\odot) \quad (1)$$

where the hats indicate true, underlying quantities – as opposed to the noisy, observable quantities L_X and M_{BH} .

This is equivalent to considering the dependence of the average Eddington-scaled X-ray luminosity with black hole mass: $\langle L_X/M_{\text{BH}} \rangle \propto \langle L_X/L_{\text{Edd}} \rangle \propto M_{\text{BH}}^\beta$, where $\beta = (1 - B)$. We assume errors $\sigma_M = 0.44$ dex on the logarithm of the black hole mass (Gültekin et al. 2009), 30% uncertainty on the measured X-ray luminosities, and use this to define Gaussian likelihood functions, $P_r(M_{\text{BH}}|\hat{M}_{\text{BH}})$ and $P_r(L_X|\hat{L}_X)$. For the non-detections, $P_r(L_X|\hat{L}_X)$ is taken to be Gaussian for luminosities higher than our limiting threshold, and uniform for all luminosities less than the limit.

We include intrinsic scatter σ_0 on the luminosity as a free parameter as well, via a Gaussian probability density function (PDF) $P_r(\hat{L}_X|\hat{M}_{\text{BH}})$. We assign scale-invariant Jeffreys priors both for this parameter and also the power law normalization (see e.g. Sivia 2006). For the power law index B , we note that this is a gradient on a log-log plot, and, in the absence of any causal connection between L_X and M_{BH} , we assign a prior to enforce rotational invariance, which is equivalent to retaining ambivalence as to whether we are seeing an L_X - M_{BH} relation, or rather a M_{BH} - L_X relation.

This results in the following PDF:

$$P_r(B) \propto (1+B^2)^{-3/2}. \quad (2)$$

Having defined these distributions, we then, at any given position in $\{A, B, \sigma\}$ space, integrate out each of the $i = 100$ nuisance parameters $\hat{M}_{\text{BH},i}$. This operation is equivalent to convolving the intrinsic spread with the error distributions:

$$P_r(L_{X,i}|M_{\text{BH},i}, A, B, \sigma_0) = \frac{\exp\left[-\frac{(\log L_X - B \log M_{\text{BH}} - A)^2}{2(\sigma_0^2 + \sigma_{L,i}^2 + B^2 \sigma_{M,i}^2)}\right]}{\sqrt{(2\pi)(\sigma_0^2 + \sigma_{L,i}^2 + B^2 \sigma_{M,i}^2)}} \quad (3)$$

where σ_L denotes the error on $\log L_X$. This marginalization requires a prior to be assigned for the \hat{M}_{BH} parameters: we used a uniform distribution in $\log(\hat{M}_{\text{BH}})$, which corresponds to a power-law mass function of index -1 (see e.g. Greene & Ho 2007, 2009 for comparison).

We explore the $\{A, B, \sigma\}$ parameter space using a Markov Chain Monte-Carlo sampler, the output of which is a set of samples that characterize the desired posterior PDF $P_r(A, B, \sigma|\{L_X, M_{\text{BH}}\})$. We ran multiple chains to ensure convergence. The fit is illustrated in Figure 4, where we show the (median) intrinsic scatter about the (median) relation, while the posterior distribution is shown in Figure 5, where we have marginalized over the normalization A . We find the index $B = 0.38^{+0.13}_{-0.12}$, while the scatter is inferred to be $\sigma_0 = 0.46^{+0.08}_{-0.06}$ dex (68% confidence intervals around the one-dimensional marginalised PDF median values).

A zero slope, corresponding to no dependence of L_X on M_{BH} , is ruled out at high confidence: $P_r(B = 0.0) \simeq 0.001$. Likewise, a slope of unity, corresponding to no dependence of L_{Edd} on M_{BH} , is also rejected: $P_r(B = 1.0) \lesssim 10^{-4}$. In terms of Eddington ratio, the relation in Equation 1 still becomes: $\langle L_X/L_{\text{Edd}} \rangle \propto M_{\text{BH}}^{-0.62}$, that is, on average, *low mass black holes seem to be more active (i.e. emit closer to their Eddington limits) than higher mass objects*. As a consequence – pending the large uncertainties on the black holes’ mass function (see Greene & Ho 2007, 2009) and occupation fraction (see Volonteri et al. 2008; Van Wassenhoven et al. 2010) in the local universe – the active fraction, here defined as above a certain Eddington ratio, is a decreasing function of M_{BH} .

As how to the average Eddington-scaled X-ray luminosity (and hence the active fraction) might depend on M_* , this is obviously related to the scaling of M_{BH} with M_* (such a scaling is somewhat expected, albeit with a much larger scatter, as a result of the observed relation between M_{BH} and bulge mass). Specifically, for the black holes in our sample of active SMBHs, $M_{\text{BH}} \propto M_*^\delta$, with $\delta = 1.2 \pm 0.6$ (assuming a scatter of 0.44 dex for both). Owing to the extremely large scatter, this could still be marginally consistent with no dependence of L_{Edd} (hence of the active fraction) on stellar mass, i.e.: $\langle L_X/L_{\text{Edd}} \rangle \propto M_*^{-0.8 \pm 0.5}$ (68% C.L.).

5. THE X-RAY LUMINOSITY FUNCTION

The differential logarithmic X-ray luminosity function (XLF) of the active SMBHs in the AMUSE-Virgo sample is well approximated by the following expression:

$$\frac{dN}{d \ln L_X} = K_{\text{AMUSE}} \left(\frac{L_X}{10^{38} \text{ erg s}^{-1}} \right)^{-\Gamma_{\text{AMUSE}}} \quad (4)$$

where the best-fit parameters are: $K_{\text{AMUSE}} = 1.4 \pm 0.1$, and $\Gamma_{\text{AMUSE}} = 0.4 \pm 0.1$. For comparison, the differential XLF of off-nuclear LMXBs, as given by Gilfanov (2004), is well approximated by a power law with two breaks, having negative differential slopes¹⁴ $\beta_1 = 1.86 \pm 0.12$ between $0.2 - 5.0 \times 10^{38}$

¹⁴ Defined as $\beta = (\Gamma + 1)$.

erg s⁻¹, and $\beta_2 = 4.8 \pm 1.1$ above 5×10^{38} erg s⁻¹, while its normalization scales with the stellar mass of the host galaxy (see also: Kim & Fabbiano 2004; Humphrey & Buote 2004). A visual comparison between the two XLFs is also shown in Figure 6: plotted are the fitted XLF for the nuclear X-ray sources in the AMUSE sample (red histogram) and the functional expression for the LMXB XLF (Gilfanov 2004), scaled to a stellar mass of $10^{11} M_\odot$. On average, this normalization corresponds to conservatively assuming that the *Chandra* PSF at the distance of Virgo encloses about 2% of the stellar mass of each galaxy. The fitted XLF slope is much shallower for the AMUSE sample than for the extragalactic LMXBs, further strengthening our conclusion that contamination from stellar mass objects has been properly accounted for. In addition, we recover a similar slope to that reported by Zhang et al. (2009) for a sample of 86 nearby (within 15 Mpc) galaxies hosting a nuclear X-ray source: the fitted slope for their sample is 0.5, i.e. consistent, within the errors, with our results. We argue though that the Zhang et al. sample might suffer from a slight contamination from X-ray binaries at the low mass end, given that it includes both early and late type galaxies – with the latter ones having an enhanced contamination from bright high-mass X-ray binaries.

6. DISCUSSION

6.1. Super-massive black holes vs. massive nuclear star clusters

Until recently it was generally believed that massive black holes and nuclear star clusters did not generally coexist at the centres of galaxies. Less than a handful of counter-examples (e.g. Filippenko & Ho 2003; Graham & Driver 2007) were the exceptions to confirm the rule. More systematic studies, e.g. by Ferrarese et al. (2006a) and Wehner & Harris (2006), showed the transition between galaxies which host predominantly a black hole vs. a nuclear cluster occurs around $10^{10} M_\odot$. However, while the latter conclude that nucleated galaxies show no evidence of hosting SMBHs, the former speculate that nuclei form in all galaxies but they are destroyed by the evolution of preexisting SMBHs or collapse into a SMBH in the most massive cases. It is also suggested that “SMBHs and nuclei are almost certainly mutually exclusive in the faintest galaxies belonging to the VCS sample¹⁵”. This is indicated by the fact that, although the nuclear masses of NGC 205 and M33 are fully consistent with the relation¹⁶ between the mass the nuclear object (be it a cluster or a BH) and the host galaxy, the upper limits on their SMBH masses are not, implying that “[...] neither galaxy contains an SMBH of the sort expected from extrapolations of the scaling relations defined by SMBHs in massive galaxies”. Merritt (2009) examines the evolution of nuclear star clusters with and without SMBHs from a theoretical point of view, finding that nuclear star clusters with black holes are always bound to expand, due primarily to heating from the galaxy and secondarily to heating from stellar disruptions. As a consequence, core-collapsed clusters should not be harboring nuclear black holes.

From an observational point of view, there has been a number of efforts to quantify the degree of coexistence of nuclear clusters and SMBHs, and their mutual properties. Seth et al. (2008) searched for active nuclei in 176 galaxies with known nuclear clusters, using optical spectroscopy, X-ray and radio

data. They find that the AGN fraction increases strongly with increasing galaxy and nuclear cluster mass, consistent with previous studies of the general galaxy population. In addition, the variation of the AGN fraction with Hubble type is also consistent with the whole Palomar sample (Ho et al. 1997), indicating that the presence (or absence) of a nuclear star cluster does not play a crucial role in boosting (or hampering) accretion-powered activity onto a SMBH (see also Gonzalez-Delgado et al. 2008). More recently, Graham & Spitler (2009) reported on 12 new systems which host both a nuclear star cluster and a SMBHs, and for which they were able to acquire both the masses of the nuclear components, as well as the stellar mass of the host spheroid. They find that, for host stellar masses in the range 10^8 – $10^{11} M_\odot$, the nucleus-to-spheroid mass ratio decreases from a few to about 0.3%. This ratio is expected to saturate to a constant value once dry merging commences, and the nuclear cluster disappears. Our work tackles the issue of nuclear SMBH-star cluster coexistence taking a complementary approach with respect to that of Seth et al., that is, we ask how many of those nuclei which show a nuclear cluster also host a (X-ray active) SMBH. We remind the reader that the VCS sample (Côté et al. 2004) surveyed by AMUSE-Virgo is complete down to a *B* magnitude of -18 , and is a random sample of fainter (early type) objects. In terms of (hosts’) stellar mass distribution, the sample peaks well below $10^{11} M_\odot$, and is thus particularly well suited for investigating hybrid potentially nuclei. While 32 out of 100 galaxies are found to host a nuclear X-ray source, only 6 of them also show evidence for a nuclear star cluster as visible from archival *Hubble* images (typically, the star clusters are identified as overdensities above a single-component Sersic profile, but see Ferrarese et al. 2006b for details about the fitting procedure). After taking into account LMXB contamination, while the fraction of hybrid nuclei as function of host stellar mass M_* is constrained between 0.3 and 7% for $\log M_* > 11$ (95% C.L., and down to a limiting 2–10 keV luminosity of $\sim 2 \times 10^{38}$ erg s⁻¹), the lack of star cluster–SMBH matches above 10^{11} sets an upper limit of 32% to the fraction of such hybrid nuclei in massive early types.

6.2. Active fraction and down-sizing in black hole accretion

The bottom panel of Figure 2 shows how the fraction f_X of objects hosting an active SMBH –down to our luminosity limit– increases as a function of the host mass M_* : $0.01 < f_X < 0.14$ for $\log(M_*/M_\odot) < 9.5$, $0.53 < f_X < 0.87$ for $\log(M_*/M_\odot) > 10.5$, and $0.16 < f_X < 0.43$ for intermediate masses. While this result is fully consistent with earlier works (Ho et al. 1997; Decarli et al. 2007; Kauffmann et al. 2003; Seth et al. 2008; Satyapal et al. 2008; Gallo et al. 2008), this is not to say that the fraction of objects which host an active SMBH raises with mass tout-court. As discussed in § 4.1, dealing with a sample that is ‘Eddington-limited’, rather than simply luminosity-limited, results in no observational evidence for a statistically significant increase in the active SMBH fraction with mass (either host galaxy’s or BH’s). The same test as above can be applied to hybrid nuclei: after considering sub-samples complete down to Eddington ratios between 10^{-6} and 10^{-9} , we conclude that the number of nuclei hosting both an active SMBH and a massive star cluster does not show a trend of increasing incidence with increasing host stellar mass. It must be stressed, however, that restricting the analysis to ‘Eddington-complete’ sub-samples results in very large error bars.

¹⁵ The same considered in this work.

¹⁶ See Figure 2 in Ferrarese et al. (2006a).

A more quantitative constraint can be obtained through a Bayesian approach to infer a dependence between the measured X-ray luminosities and black hole masses (4.2). This analysis highlights, for the first time, a dependence of accretion-powered X-ray luminosity on black hole mass. A slope $B = 0.38^{+0.13}_{-0.12}$ in Equation 1 implies that the average Eddington scaled X-ray luminosity scales with black hole mass to the power -0.62 . As a consequence, *the local active fraction*— defined as those above a fixed X-ray Eddington ratio— *decreases with black hole mass* (as well as with host stellar mass, as long as a positive relation holds between those two quantities). This can be considered as the analogous of galaxy ‘down-sizing’ (cf. Cowie et al. 1996) in the context of black hole accretion: within the local universe, low mass SMBHs emit closer to their Eddington limit than high mass objects. On the same line, using a combination of SDSS and Galaxy Zoo data within $z = 0.05$, Schawinski et al. (2010) find evidence for a dependence of the black hole growth on the host galaxy morphology: while late-type galaxies host preferentially the most massive black holes, early-type galaxies host preferentially low mass black holes. More specifically, for (bolometric) Eddington-scaled luminosities in excess of 10%, low mass early type galaxies are the only population to host a substantial fraction of active SMBHs, in qualitative agreement with our findings (albeit at higher luminosities).

A second interesting result is that, within the VCS sample surveyed by AMUSE-Virgo, the distribution of Eddington-scaled luminosities of the detected nuclei turns out to be very broad, in contrast with what reported for higher redshift *bona fide* AGN. In fact, Figure 3 indicates no clear cut in terms of active SMBH luminosity: as stated at the beginning of this Paper, the distinction between active and inactive is rather arbitrary, and is ultimately set by our ability to detect and interpret signatures of accretion-powered activity. In principle, X-rays due to non-thermal processes in the vicinity of a BH offer clear-cut diagnostics of accretion-powered activity. However, as illustrated in Table 2. already at the distance of Virgo, the chance contamination to the nuclear X-ray emission from LMXBs is substantial, even with the fine spatial resolution of *Chandra*. X-ray surveys of ‘inactive’ galaxies are necessarily limited by this contamination; the problem is only marginally alleviated with deeper exposures, since the 0.5-10 keV spectrum of a luminous X-ray binary is virtually undistinguishable from that of a highly sub-Eddington SMBHs. As the distance increases so does the mass enclosed with the X-ray instrument PSF, and thus the chance of having a number of medium luminosity X-ray binaries ‘mimicking’ a low luminosity AGN. While X-rays alone can not possibly provide us with a clean answer as to the nature of the nuclear accretors, the picture may clarify when the high energy properties are interpreted in concert with other wavelength’s. In particular, mid-infrared emission can be a sensitive tracer of accretion-powered emission from a massive accretor: while X-ray binaries emit the bulk of their energy in the X-ray band, SMBHs accretion-powered emission ought to peak at lower frequencies, thus representing a potential source of heating for local dust to re-process. Additionally, sensitive mid-IR observation may unveil obscured accretion-powered emission due to the presence of e.g. a dust lane/dusty torus. This will be explored in detail by comparing the mid-IR (24 μm *Spitzer* observations) radial profiles of the AMUSE-Virgo

galaxies with the smoothed optical profiles from *Hubble* (Leipski et al. , Paper III., in preparation).

The notion that energy feedback from super-massive black holes could solve a number of problems faced by the hierarchical paradigm at galactic scales has been substantiated by a number of recent works: the vast majority of AGN at $z \simeq 1$ occupy a rather distinct region of color-magnitude diagram, typically associated with the end of the star-forming phase (the so called “green valley”; e.g. Schawinski et al. 2007, 2009; Salim et al. 2007; Nandra et al. 2007; Silverman et al. 2008; Bundy et al. 2008; Georgakakis et al. 2008). It is also well known that environment plays an important role in regulating the gas supply in galaxies, and as a consequence their star formation rate and morphologies, via a variety of processes including high speed interactions, mergers, ram-pressure stripping. It has often been proposed that galaxy mergers and interactions also regulate fueling of the central SMBH. Although the situation remains controversial, progress is being made regarding the role of environment in regulating activity at high Eddington ratios. For example, observations of large samples of optically-selected AGN from SDSS show evidence that the luminous optically active AGN are associated with young stellar populations (Kauffmann et al. 2003; Choi et al. 2009). At the extreme end, this scenario is supported by observations of ultra-luminous infrared galaxies, that are in general associated with galaxy mergers, and have bolometric luminosities similar to quasars. High resolution numerical simulations (Springel, Di Matteo & Hernquist 2005; Ciotti & Ostriker 2007) show that the AGN activity remains obscured during most of the starburst and AGN activity phase. Sub-millimeter observations of samples of absorbed vs. unabsorbed AGN have consistently confirmed this picture (e.g. Page et al. 2004; see also Alexander et al. 2008).

In contrast to this, low-luminosity radio-loud AGN in the nearby universe are seen to be preferentially hosted by massive elliptical galaxies, which tend to be found in richer environments, where gas-rich galaxy mergers are less likely to occur. Comprehensive studies are underway to characterize the AGN populations in clusters vs field as a function of cosmic time. However, very little is known about the environmental dependency of nuclear activity at low levels. Given the suggested role of low levels of nuclear activity in regulating star formation, the discovery of environmental trends would have profound implications not only for understanding black hole growth but also for understanding galaxy formation and evolution. This issue will be tackled through an approved *Chandra* program (Cycle 11) targeting 100 early type field galaxies within 30 Mpc.

7. AMUSE-VIRGO. II: SUMMARY

With the goal of providing an unbiased census of local SMBH activity in early type galaxies, the AMUSE-Virgo survey targets an homogeneous sample of 100 nearby galaxies with the *Chandra* X-ray Observatory and the *Spitzer Space Telescope* down to a limiting threshold of L_{Edd} for a $3 M_{\odot}$ object ($3\text{-}\sigma$). The targeted sample is that of the *Hubble* Virgo Cluster Survey (VCS; Côté et al. 2004). For each galaxy, the high resolution g and z band images enable us to resolve, when present, the nuclear star cluster, infer its enclosed mass, and thus estimate the chance contamination from a low-mass X-ray binary (LMXB) as bright/brighter than the detected X-ray core. The main results and implications of this work can

be summarized as follows:

1. Out of 100 objects, 32 show a nuclear X-ray source. After carefully accounting for contamination from LMXBs, making use of their X-ray luminosity function in external galaxies, we are able to conclude that between 24–34% of the galaxies in our sample host a X-ray active SMBH, down to our limiting X-ray luminosity (at the 95% C.L.). This sets a firm lower limit to the black hole occupation fraction in nearby bulges within a cluster environment.
2. As already reported in Paper I. of this series, we confirm that the fraction f_X of active nuclear SMBHs is an increasing function of the host stellar mass M_* , with $0.01 < f_X < 0.14$ for $\log(M_*/M_\odot) < 9.5$, $0.53 < f_X < 0.87$ for $\log(M_*/M_\odot) > 10.5$, and $0.16 < f_X < 0.43$ for intermediate masses (Figure 2). While this trend of (fractionally) increasing nuclear SMBH activity with increasing galaxy mass is well known, here we are able to show that it simply results from dealing with a luminosity-limited survey instead of a ‘Eddington-limited’ one.
3. Only 6/100 objects host both a nuclear star cluster and a nuclear X-ray source; of those 6, 2 are likely to be heavily contaminated by LMXB X-ray emission. After accounting for this effect, the fraction of such hybrid nuclei is constrained between 0.3–7% for host stellar masses below $10^{11} M_\odot$, and to be lower than 32% above it (95% C.L.).
4. The differential logarithmic X-ray luminosity function of active SMBHs in our sample scales with the X-ray luminosity as $L_X^{-0.4 \pm 0.1}$ between a few 10^{38} and 10^{42} erg s^{-1} . The fitted slope is much shallower than for LMXBs, confirming the different nature of the nuclear X-ray sources’ population.
5. In terms of Eddington-scaled luminosities, the inferred ratios range between a few 10^{-9} and a few 10^{-6} , much broader than what reported for high redshift AGN (e.g. Kollmeier et al. 2006). We speculate that it is likely to

extend to *bona fide* AGN, similarly to what is observed in the hard X-ray state of BH X-ray binaries.

6. We use a Bayesian statistical analysis to assess the dependence of the accretion-powered X-ray luminosity on the black hole mass, taking into account selection effects. We find that the average L_X/L_{Edd} depends on black hole mass as : $\log(L_X/10^{38} \text{ erg s}^{-1}) = A + B \log(M_{\text{BH}}/10^8 M_\odot)$, with $A = 1.0 \pm 0.1$, $B = 0.38^{+0.13}_{-0.12}$, and with an intrinsic scatter of $0.46^{+0.08}_{-0.06}$ dex. In turn, $L_X/L_{\text{Edd}} \propto M_{\text{BH}}^{-0.62 \pm 0.12}$, arguing for a ‘down-sizing’ behavior of local black hole accretion: low mass black holes shine closer to their Eddington limit than high mass ones.
7. Stacking the 64 new *Chandra* observations with no visible accreting SMBH results in a statistically significant detection of a nuclear X-ray source with average X-ray luminosity $\langle L_X/L_{\text{Edd}} \rangle \simeq 3.2 \pm 1.4 \times 10^{37}$ erg s^{-1} , consistent with emission from local LMXBs. This translates into an upper limit to the average Eddington-scaled X-ray luminosity of about 3×10^{-8} , for an average nuclear black hole mass of $10^7 M_\odot$.

E.G. is supported through Hubble Postdoctoral Fellowship grant number HST-HF-01218.01-A from the Space Telescope Science Institute, which is operated by the Association of Universities for Research in Astronomy, Incorporated, under NASA contract NAS5-26555. T.T. acknowledges support from the NSF through CAREER award NSF-0642621, by the Sloan Foundation through a Sloan Research Fellowship, and by the Packard Foundation through a Packard Fellowship. Support for this work was provided by NASA through Chandra Award Number 08900784 issued by the Chandra X-ray Observatory Center. We are grateful to Patrick Côté and Laura Ferrarese for helpful comments, and for providing us with the list of masses for the nuclear star clusters. We thank the anonymous referee for the thorough and constructive report.

REFERENCES

- Alexander, D. M., et al. 2008, *AJ*, 135, 1968
 Allen, S. W., Di Matteo, T., & Fabian, A. C. 2000, *MNRAS*, 311, 493
 Bell, E. F., McIntosh, D. H., Katz, N., & Weinberg, M. D. 2003, *ApJS*, 149, 289
 Bentz, M., et al. 2009, *ApJ*, 705, 199
 Bernardi, M., Alonso, M. V., da Costa, L. N., Willmer, C. N. A., Wegner, G., Pellegrini, P. S., Rité, C., & Maia, M. A. G. 2002, *AJ*, 123, 2990
 Blakeslee, J. P., et al. 2009, *ApJ*, 694, 556
 Bundy, K., et al. 2008, *ApJ*, 681, 931
 Canizares, C. R., Fabbiano, G., & Trinchieri, G. 1997, *ApJ*, 312, 503
 Choi, W. W., Woo, J.-H., & Park, C. 2009, *ApJ*, 699, 1679
 Ciotti, L., & Ostriker, J. P. 2007, *ApJ*, 665, 1038
 Constantin, A., Hoyle, F., & Vogeley, M. S. 2008, *ApJ*, 673, 715
 Constantin, A., & Vogeley, M. S. 2006, *ApJ*, 650, 727
 Côté, P., et al. 2007, *ApJ*, 671, 1456
 Côté, P., Piatek, S., Ferrarese, L., Jordán, A., Merritt, D., Peng, E. W., Haşegan, M., Blakeslee, J. P., Mei, S., West, M. J., Milosavljević, M., & Tonry, J. L. 2006, *ApJS*, 165, 57
 Côté, P., Blakeslee, J. P., Ferrarese, L., Jordán, A., Mei, S., Merritt, D., Milosavljević, M., Peng, E. W., Tonry, J. L., & West, M. J. 2004, *ApJS*, 153, 223
 Cowie, L. L., Songaila, A., Hu, E. M., & Cohen, J. G. 1996, *AJ*, 112, 839
 Decarli, R., Gavazzi, G., Arosio, I., Cortese, L., Boselli, A., Bonfanti, C., & Colpi, M. 2007, *MNRAS*, 381, 136
 Dickey, J. M., & Lockman, F. J. 1990, *ARA&A*, 28, 215
 Di Matteo, T., Allen, S. W., Fabian, A. C., Wilson, A. S., & Young, A. J. 2003, *ApJ*, 582, 133
 Di Matteo, T., Carilli, C. L., & Fabian, A. C. 2001, *MNRAS*, 547, 731
 Di Matteo, T., Quataert, E., Allen, S. W., Narayan, R., & Fabian, A. C. 2000, *MNRAS*, 311, 507
 Fabbiano, G., Baldi, A., Pellegrini, S., Siemiginowska, A., Elvis, M., Zezas, A., & McDowell, J. 2004, *ApJ*, 616, 730
 Fabbiano, G., Elvis, M., Markoff, S., Siemiginowska, A., Pellegrini, S., Zezas, A., Nicastro, F., Trinchieri, G., & McDowell, J. 2003, *ApJ*, 588, 175
 Fabbiano, G. 1993, *Advances in Space Research*, 12, 161
 Fabbiano, G., & Juda, J. Z. 1997, *ApJ*, 476, 666
 Ferrarese, L., Côté, P., Dalla Bontà, E., Peng, E. W., Merritt, D., Jordán, A., Blakeslee, J. P., Haşegan, M., Mei, S., Piatek, S., Tonry, J. L., & West, M. J. 2006a, *ApJ*, 644, L21
 Ferrarese, L., Côté, P., Jordán, A., Peng, E. W., Blakeslee, J. P., Piatek, S., Mei, S., Merritt, D., Milosavljević, M., Tonry, J. L., & West, M. J. 2006b, *ApJS*, 164, 334
 Ferrarese, L., & Ford, H. 2005, *Space Science Reviews*, 116, 523
 Ferrarese, L., & Merritt, D. 2000, *ApJ*, 539, L9

- Filippenko, A. V., & Ho, L. C., 2003, *ApJ*, 588, L13
- Gallo, E., Treu, T., Jacob, J., Woo, J.-H., Marshall, P. J., & Antonucci, R., 2008, *ApJ*, 680, 154 (Paper I)
- Garmire, G., Feigelson, E. D., Broos, P., Hillenbrand, L. A., Pravdo, S. H., Townsley, L., & Tsuboi, Y. 2000, *AJ*, 120, 1426
- Gebhardt, K., Kormendy, J., Ho, L. C., Bender, R., Bower, G., Dressler, A., Faber, S. M., Filippenko, A. V., Green, R., Grillmair, C., Lauer, T. R., Magorrian, J., Pinkney, J., Richstone, D., & Tremaine, S. 2000, *ApJ*, 543, L5
- Gehrels, N. 1986, *ApJ*, 303, 336
- Georgakakis, A., et al. 2008, *MNRAS*, 385, 204
- Ghosh, H. Mathur, S., Fiore, F., & Ferrarese, L. 2008, *ApJ*, 687, 216
- Gilfanov, M. 2004, *MNRAS*, 349, 146
- González Delgado, R. M., Pérez, E., Cid Fernandes, R., & Schmitt, H., 2008, *ApJ*, 135, 747
- Graham, A. W., & Spitler, L. R. 2009, *MNRAS*, 397, 2148
- Graham, A. W., & Driver, S. P. 2007, *MNRAS*, 380, L15
- Greene, J. E., & Ho, L. C. 2009 *ApJ*, 704, 1743
- Greene, J. E., & Ho, L. C. 2007, *ApJ*, 667, 131
- Gültekin, K., et al. 2009, *ApJ*, 698, 198
- Heckman, T. M., Kauffmann, G., Brinchmann, J., Charlot, S., Tremonti, C., & White, S. D. M. 2004, *ApJ*, 613, 109
- Ho, L. C. 2008, *ARA&A*, 46, 475
- Ho, L. C., Feigelson, E. D., Townsley, L. K., Sambruna, R. M., Garmire, G. P., Brandt, W. N., Filippenko, A. V., Griffiths, R. E., Ptak, A. F., & Sargent, W. L. W. 2001, *ApJ*, 549, L51
- Ho, L. C., Filippenko, A. V., & Sargent, W. L. W. 1997, *AJ*, 487, 568
- Humphrey, P. J., & Buote, D. A. 2008, *ApJ*, 689, 983
- Kauffmann, G., Heckman, T. M., & Best, P. N. 2008, *MNRAS*, 353, 713
- Kauffmann, G., et al. 2004, *MNRAS*, 353, 713
- Kauffmann, G., et al. 2003, *MNRAS*, 346, 1055
- Kewley, L. J., Groves, B., Kauffmann, G., & Heckman, T. 2006, *MNRAS*, 372, 961
- Kim, D.-W., & Fabbiano, G. 2004, *ApJ*, 611, 846
- Kollmeier, J. A., Onken, C. A., Kochanek, C. S., Gould, A., Weinberg, D. H., Dietrich, M., Cool, R., Dey, A., Eisenstein, D. J., Jannuzi, B. T., Le Floch, E., & Stern, D. 2006, *ApJ*, 648, 128
- Kormendy, J., Fisher, D. B., Cornell, M. E., & Bender, R. 2009, *ApJS*, 182, 216
- Kormendy, J., Bender, R., Magorrian, J., Tremaine, S., Gebhardt, K., Richstone, D., Dressler, A., Faber, S. M., Grillmair, C., & Lauer, T. R. 1997, *ApJ*, 482, L139
- Kormendy, J., & Richstone, D. 1995, *ARA&A*, 33, 581
- Lauer, T. R., Gebhardt, K., Faber, S. M., Richstone, D., Tremaine, S., Kormendy, J., Aller, M. C., Bender, R., Dressler, A., Filippenko, A. V., Green, R., & Ho, L. C. 2007, *ApJ*, 664, 226
- Lauer, T. R., Tremaine, S., Ajhar, E. A., Bender, R., Dressler, A., Faber, S. M., Gebhardt, K., Grillmair, C. J., Kormendy, J., & Richstone, D. 1996, *ApJ*, 471, L79
- Loewenstein, M., Mushotzky, R. F., Angelini, L., Arnaud, K. A., & Quataert, E. 2001, *ApJ*, 555, L21
- Magorrian, J., et al. 1997, *AJ*, 115, 2285
- Marconi, A., Risaliti, G., Gilli, R., Hunt, L. K., Maiolino, R., & Salvati, M. 2004, *MNRAS*, 222, 49
- Marconi, A., & Hunt, L. K. 2003, *ApJ*, 589, L21
- McLure, R. J., & Dunlop, J. S. 2002, *MNRAS*, 331, 795
- Mei, S., Blakeslee, J. P., Côté, P., Tonry, J. L., West, M. J., Ferrarese, L., Jordán, A., Peng, E. W., Anthony, A., & Merritt, D. 2007, *ApJ*, 655, 144
- Merloni, A., & Heinz, S. 2008, *MNRAS*, 388, 1011
- Miller, C. J., Nichol, R. C., Gómez, P. L., Hopkins, A. M., & Bernardi, M. 2003, *ApJ*, 597, 142
- Nandra, K., et al. 2007, *ApJ*, 660, L11
- Ott, J., Walter, F., & Brinks, E. 2005, *MNRAS*, 358, 1453
- Page, M. J., Stevens, J. A., Ivison, R. J., & Carrera, F. J. 2004, *ApJ*, 611, L85
- Pellegrini, S., Ciotti, L., & Ostriker, J. P. 2007, *ApJ*, 4, 340
- Pellegrini, S. 2005, *ApJ*, 624, 155
- Rich, R. M. 2005, *ApJ*, 619, L107
- Roberts, T. P., & Warwick, R. S. 2000, *MNRAS*, 315, 98
- Salim, S., et al. 2007, *ApJS*, 173, 267
- Santra, S., Sanders, J. S., & Fabian, A. C. 2007, *MNRAS*, 382, 895
- Sarazin, C. L., Irwin, J. A., & Bregman, J. N. 2001, *ApJ*, 556, 553
- Satyapal, S., Vega, D., Dudik, R. P., Abel, N. P., & Heckman, T. 2008, *ApJ*, 677, 926
- Schawinski, K., et al. 2010, *AJ*, in press (arXiv:1001.3141)
- Schawinski, K., Virani, S., Simmons, B., Urry, C. M., Treister, E., Kaviraj, S., & Kushkuley, B. 2009, *ApJ*, 692, L19
- Schawinski, K., et al. 2007, *MNRAS*, 382, 1415
- Seth, A., et al. 2010, *AIP Conf. Series*, in press (arXiv:1002.0824)
- Seth, A., Agüeros, M., Lee, D., & Basu-Zych, A. 2008, *ApJ*, 678, 116
- Shankar, F., Weinberg, D. H., & Miralda-Escudé, J. 2009, *ApJ*, 690, 20
- Silverman, J. D., et al. 2008, *ApJ*, 675, 1025
- Sivakoff, G. R., Jordán, A., Sarazin, C. L., Blakeslee, J. P., Côté, P., Ferrarese, L., Juett, A. M., Mei, S., & Peng, E. W. 2007, *ApJ*, 660, 1246
- Sivia, D. S. 2006, *Data Analysis, A Bayesian Tutorial*, Oxford University Press (Oxford)
- Soltan, A. 1982, *MNRAS*, 200, 115
- Soria, R., Graham, A. W., Fabbiano, G., Baldi, A., Elvis, M., Jerjen, H., Pellegrini, S., & Siemiginowska, A. 2006a, *ApJ*, 640, 143
- Soria, R., Graham, A. W., Fabbiano, G., Baldi, A., Elvis, M., Jerjen, H., Pellegrini, S., & Siemiginowska, A. 2006b, *ApJ*, 640, 126
- Springel, V., Di Matteo, T., & Hernquist, L. 2005, *MNRAS*, 361, 776
- Terashima, Y., & Wilson, A. S. 2003, *ApJ*, 583, 145
- Tremaine, S., Gebhardt, K., Bender, R., Bower, G., Dressler, A., Faber, S. M., Filippenko, A. V., Green, R., Grillmair, C., Ho, L. C., Kormendy, J., Lauer, T. R., Magorrian, J., Pinkney, J., & Richstone, D. 2002, *ApJ*, 574, 740
- Valluri, M., Ferrarese, L., Merritt, D., & Joseph, C. L. 2005, *ApJ*, 628, 137
- Van Wassenhoven, S., Volonteri, M., Walker, M. G., & Gair, J. R. 2010, *MNRAS* submitted (arXiv:1001.5451)
- Volonteri, M., Haardt, F., & Gültekin, K. 2008, *MNRAS*, 384, 1387
- Wehner, E. H., & Harris, W. E., 2006, *ApJ*, 644, L17
- Woo, J.-H., & Urry, C. M. 2002, *ApJ*, 579, 530
- Yu, Q., & Tremaine, S. 2002, *MNRAS*, 335, 965
- Zhao, P., Grindlay, J. E., Hong, J. S., Laycock, S., Koenig, X. P., Schlegel, E. M., & van den Berg, M. 2005, *ApJS*, 161, 429
- Zhang, W. M., Soria, R., Zhang, S. N., Swartz, D. A., & Liu, J. F. 2009, *ApJ*, 699, 281

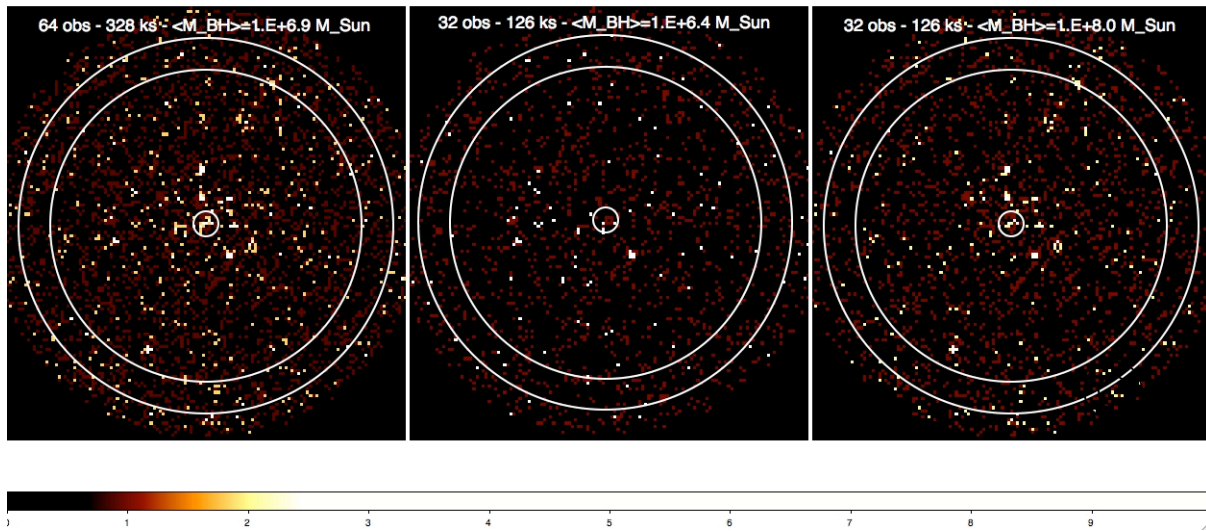


FIG. 1.— Stacking undetected nuclei. *Left:* The inner $35''$ apertures of 64 AMUSE-Virgo galaxies with undetected X-ray cores have been stacked to give a single, 328 ks ACIS-S image. A nuclear X-ray source is significantly detected in the stacked image, with net count rate of $1.1 \pm 0.2 \times 10^{-4} \text{ count s}^{-1}$. The corresponding average X-ray luminosity is consistent with what expected from nuclear LMXBs within the *Chandra* PSF.

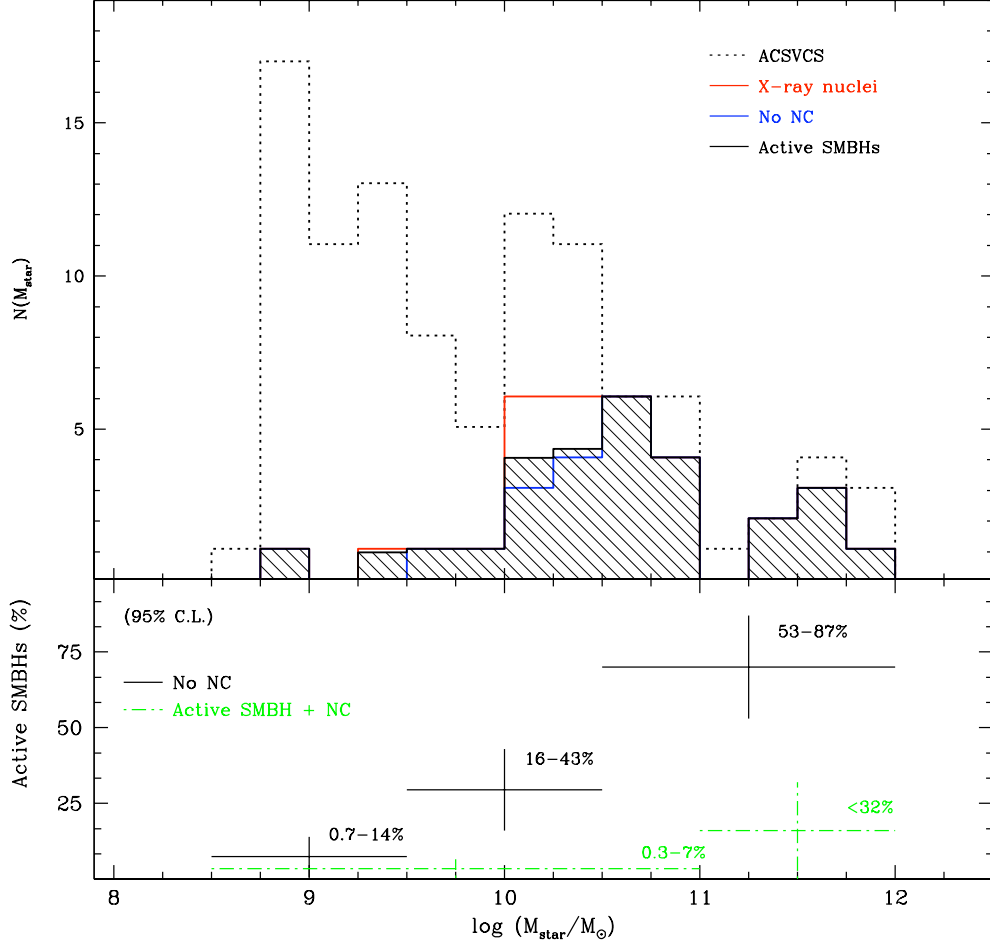


FIG. 2.— The top panel illustrates the distribution of the 100 galaxies targeted by AMUSE-Virgo (the ACSVCS sample) as a function of the host stellar mass: The dotted histogram represents the whole sample; the red histogram is for the 32 galaxies found to host X-ray cores, while the blue histogram is for the 26 X-ray cores that host no nuclear star cluster. The 6 galaxies which host hybrid nuclei have a higher chance contamination to the nuclear X-ray emission from LMXBs. The ‘weighted’ distribution of galaxies hosting an accreting SMBH is illustrated by the black shaded histogram (see § 3). The bottom panel shows the active SMBH fraction (solid black line), and the fraction of hybrids (dot-dashed green line) as a function of the host stellar mass. Numbers at given at the 95% confidence level.

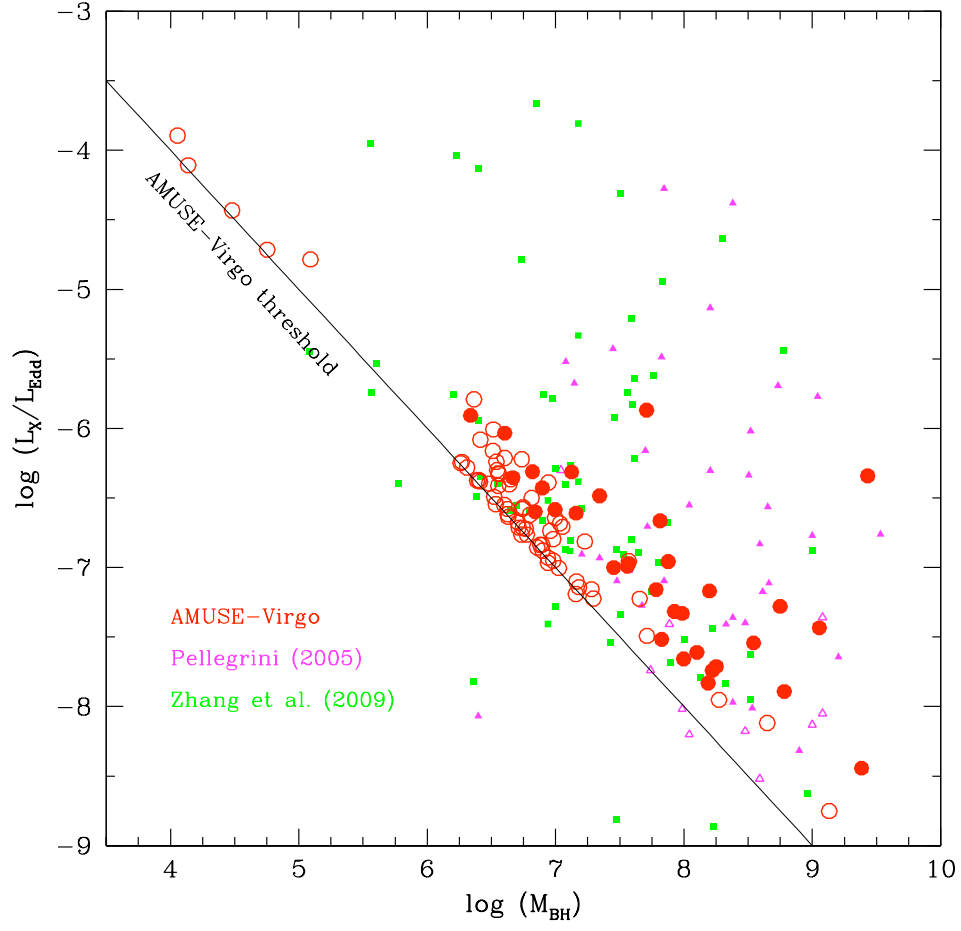


FIG. 3.— The results from AMUSE-Virgo, in red, are compared to those presented by Pellegrini (2005) and Zhang et al. (2009), in magenta and green, respectively. Open marks represents upper limits, while filled marks are for detections. Undetected nuclei from AMUSE-Virgo (open red circles) which are not ‘collapsed’ onto the *Chandra* detection threshold for our survey indicate only marginal detections (less than 6 photons were detected within a radius of $2''$ centered on the optical position).

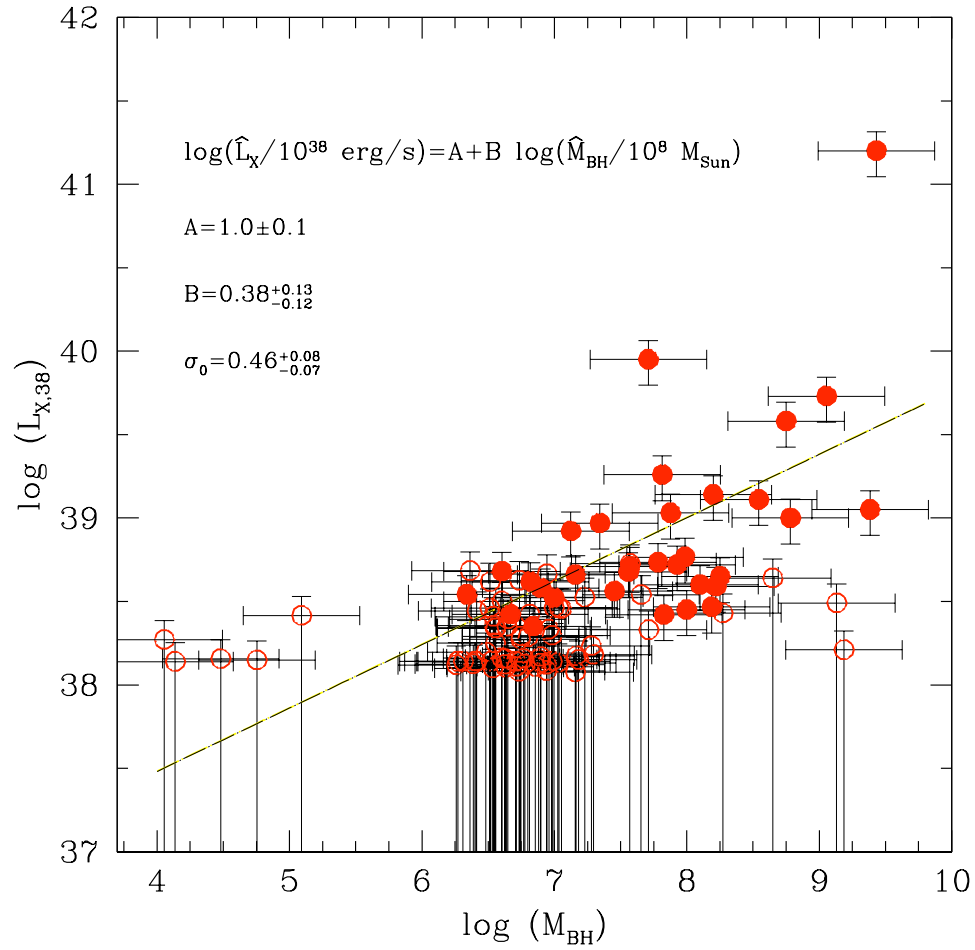


FIG. 4.— Inferred X-ray luminosities/limits for the 100 AMUSE Virgo galaxies, plotted as a function of the nuclear black hole mass. The maximum likelihood analysis presented in § 4.2 shows evidence for a correlation of the form: $\langle L_X \rangle \propto \langle M_{\text{BH}} \rangle^{0.38}$, implying that the average Eddington scaled X-ray luminosity scales with M_{BH} to the power -0.62 . This argues for a ‘down-sizing’ in black hole accretion.

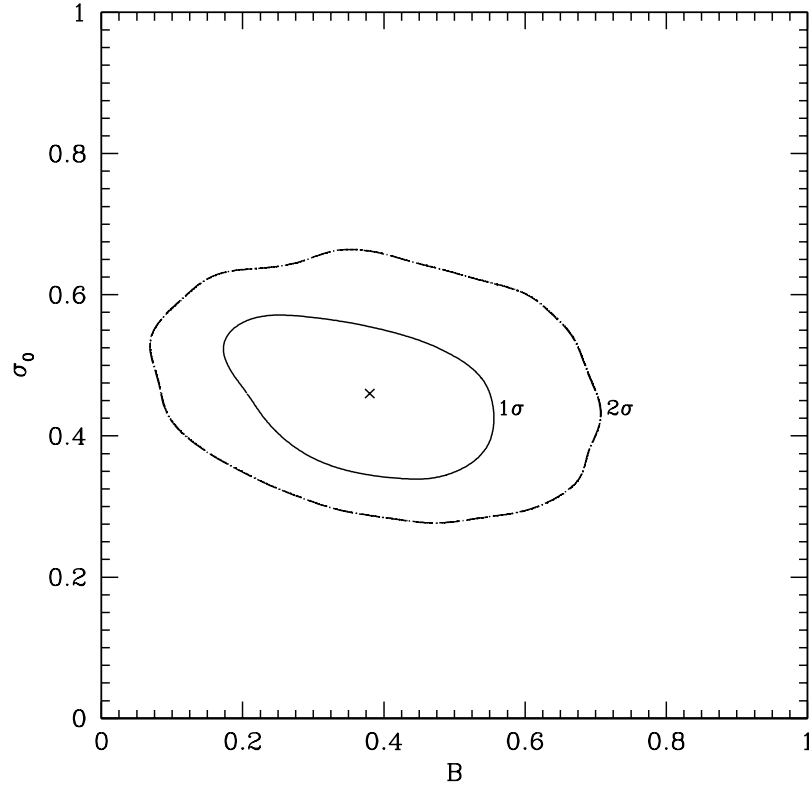


FIG. 5.— Plotted are the 68 and 95 per cent C.L. contours for the slope B and intrinsic scatter σ_0 which characterize the posterior PDF $P_r(A, B, \sigma | \{L_X, M_{\text{BH}}\})$ (defined in § 4.2, Eq. 1), marginalized over the normalization A . The inferred power law relation between the average X-ray luminosity and black hole mass is of the form: $\log(\langle L_X \rangle / 10^{38} \text{ erg s}^{-1}) = A + B \log(\langle M_{\text{BH}} \rangle / 10^8 M_\odot)$, with $A = 1.0 \pm 0.1$, $B = 0.38^{+0.13}_{-0.12}$, and with an intrinsic scatter of $0.46^{+0.08}_{-0.06}$ dex.

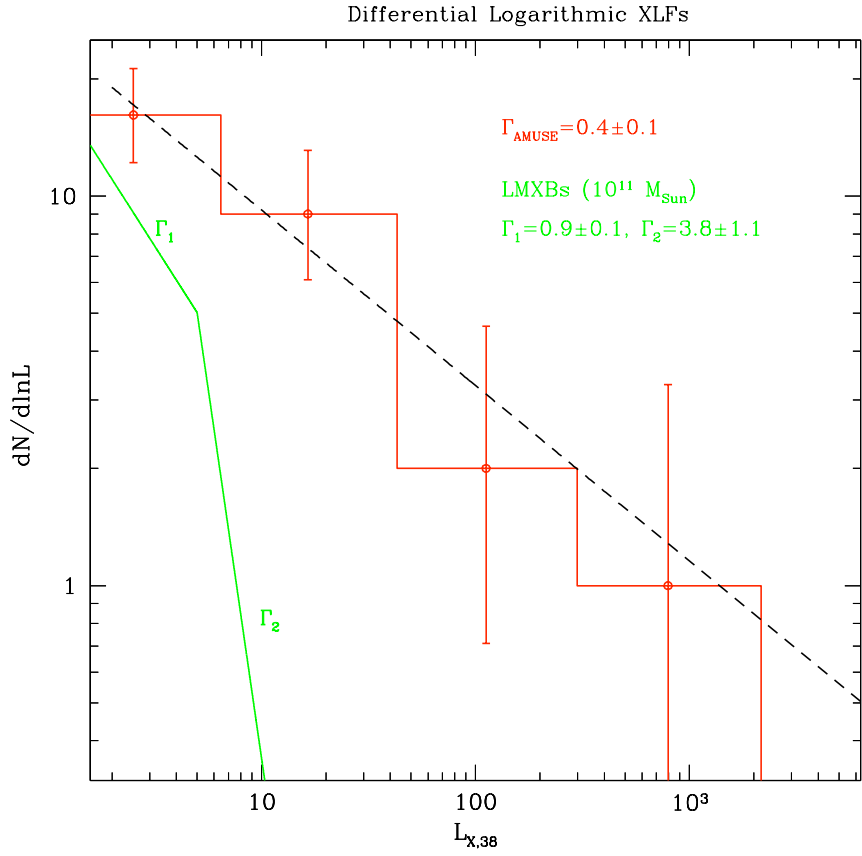


FIG. 6.— *Left*: The differential logarithmic X-ray luminosity function (XLF) of the accreting SMBHs in AMUSE-Virgo, here shown in red, is compared to the analytic expression for the field LMXB luminosity function given by Gilfanov (2004), in green, with a normalization corresponding to a stellar mass of $10^{11} M_{\odot}$. The AMUSE-Virgo XLF is well approximated by a power-law with slope $\Gamma = 0.4 \pm 0.1$, much shallower than the slope of the field LMXB XLF at the high luminosity end; this confirms the different physical nature of detected X-ray cores.

TABLE 1
AMUSE-VIRGO II.: NUCLEAR PROPERTIES.

ID	VCC	Other	d	B	σ	$\log M_{\text{BH}}$	$\log L_X$	$\log M_*$
(1)	(2)	(3)	(Mpc)	(mag)	(km s^{-1})	($\log M_{\odot}$)	[$\log(\text{erg s}^{-1})$]	($\log M_{\odot}$)
(1)	(2)	(3)	(4)	(5)	(6)	(7)	(8)	(9)
1	1226	M49,N4472	17.14	8.63	308 ± 9	9.1	< 38.49	12.0
2	1316	M87,N4486	17.22	9.05	355 ± 8	9.4	41.20	11.8
3	1978	M60,N4649	17.30	9.33	347 ± 9	9.4	39.05	11.7
4	881	M86,N4406	16.83	8.77	245 ± 11	8.6	< 38.64	11.9
5	798	M85,N4382	17.86	9.30	205 ± 8	8.3	< 38.43	11.6
6	763	M84,N4374	18.45	9.35	297 ± 7	9.1	39.73	11.7
7	731	N4365	23.33	9.99	261 ± 7	8.8	39.00	11.7
8	1535	N4526	16.50	10.52	316 ± 7	9.2	< 38.21	11.0
9	1903	M59,N4621	14.93	10.02	233 ± 7	8.5	39.11	11.3
10	1632	M89,N4552	15.85	10.13	257 ± 18	8.7	39.58	11.3
11	1231	N4473	15.28	11.19	189 ± 10	8.1	38.60	10.8
12	2095	N4762	16.50	11.97	147 ± 10	7.6	38.71	10.6
13	1154	N4459	16.07	11.07	170 ± 12	7.9	39.03	10.9
14	1062	N4442	15.28	11.32	197 ± 15	8.2	38.47	10.7
15	2092	N4754	16.14	11.36	200 ± 10	8.2	38.59	10.9
16	369	N4267	15.85	12.39	165 ± 11	7.8	39.26	10.4
17	759	N4371	16.98	11.55	129 ± 6	7.3	< 38.18	10.8
18	1692	N4570	17.06	11.91	180 ± 18	8.0	38.45	10.6
19	1030	N4435	16.75	11.75	174 ± 16	7.9	38.72	10.8
20	2000	N4660	15.00	11.93	203 ± 5	8.3	38.65	10.4
21	685	N4350	16.50	11.83	198 ± 9	8.2	39.14	10.6
22	1664	N4564	15.85	11.85	157 ± 9	7.7	39.95	10.6
23	654	N4340	16.50	12.22	112 ± 3	7.0	< 38.46	10.4
24	944	N4417	16.00	12.06	125 ± 4	7.2	< 38.53	10.4
25	1938	N4638	17.46	12.01	132 ± 10	7.3	38.97	10.5
26	1279	N4478	16.98	12.21	147 ± 6	7.6	< 38.73	10.5
27	1720	N4578	16.29	12.01	153 ± 15	7.7	< 38.54	10.4
28	355	N4262	15.42	12.29	179 ± 22	8.0	38.77	10.3
29	1619	N4550	15.49	12.37	93 ± 5	6.6	38.68	10.2
30	1883	N4612	16.60	12.01	104 ± 11	6.8	38.35	10.4
31	1242	N4474	15.56	12.38	93 ± 7	6.6	< 38.50	10.3
32	784	N4379	15.85	12.44	103 ± 5	6.8	38.62	10.3
33	1537	N4528	15.85	12.73	112 ± 9	7.0	38.52	10.1
34	778	N4377	17.78	12.87	139 ± 17	7.5	38.56	10.2
35	1321	N4489	15.42	12.51	...	7.7	< 38.33	10.1
36	828	N4387	17.95	12.93	99 ± 4	6.7	< 38.63	10.2
37	1250	N4476	17.62	12.63	...	7.8	38.73	10.2
38	1630	N4551	16.14	12.74	102 ± 5	6.8	< 38.29	10.2
39	1146	N4458	16.37	12.95	110 ± 8	7.0	< 38.33	10.0
40	1025	N4434	22.44	12.87	119 ± 6	7.1	38.92	10.4
41	1303	N4483	16.75	12.94	106 ± 10	6.9	< 38.15	10.1
42	1913	N4623	17.38	13.16	89 ± 10	6.5	< 38.46	10.1
43	1327	N4486A	18.28	13.25	...	7.6	38.68	10.1
44	1125	N4452	16.50	13.07	114 ± 7	7.0	< 38.46	9.9
45	1475	N4515	16.60	13.28	91 ± 10	6.6	< 38.34	9.9
46	1178	N4464	15.85	13.32	121 ± 25	7.2	38.66	9.9
47	1283	N4479	17.38	13.25	82 ± 7	6.3	38.54	10.1
48	1261	N4482	18.11	13.52	45 ± 0	5.1	< 38.42	9.8
49	698	N4352	18.71	13.28	85 ± 8	6.4	< 38.44	10.0
50	1422	I3468	15.35	13.82	...	7.2	< 38.08	9.6
51	2048	I3773	16.50	14.04	79 ± 5	6.3	< 38.12	9.6
52	1871	I3653	15.49	14.36	...	6.9	< 38.08	9.5
53	9	I3019	17.14	14.01	...	7.2	< 38.15	9.7
54	575	N4318	22.08	11.69	95 ± 4	6.6	< 38.39	10.8
55	1910	I809	16.07	14.34	...	7.0	< 38.30	9.5
56	1049	U7580	16.00	14.93	...	6.7	< 38.08	9.0
57	856	I3328	16.83	14.50	34 ± 1	4.5	< 38.16	9.5
58	140	I3065	16.37	14.28	...	7.0	< 38.13	9.4
59	1355	I3442	16.90	14.65	...	6.9	38.58	9.4
60	1087	I3381	16.67	14.11	38 ± 1	4.8	< 38.15	9.6
61	1297	N4486B	16.29	14.15	166 ± 8	7.8	38.42	9.7
62	1861	I3652	16.14	14.45	...	6.9	< 38.12	9.5
63	543	U7436	15.70	14.34	27 ± 0	4.1	< 38.27	9.4
64	1431	I3470	16.14	14.44	...	6.9	< 38.66	9.5
65	1528	I3501	16.29	14.57	...	6.9	< 38.13	9.3
66	1695	I3586	16.52	14.40	...	7.0	< 38.14	9.5
67	1833	...	16.22	14.66	...	6.9	< 38.11	9.3
68	437	U7399A	17.14	14.05	...	7.2	< 38.17	9.6
69	2019	I3735	17.06	14.68	...	6.9	< 38.17	9.4
70	33	I3032	15.07	15.23	...	6.6	< 38.25	8.9
71	200	...	18.20	15.01	...	6.8	< 38.42	9.2
72	571	...	23.77	15.02	...	7.1	< 38.46	9.4
73	21	I3025	16.50	15.04	...	6.7	< 38.11	9.0

TABLE 1 — *Continued*

ID	VCC	Other	d (Mpc)	B (mag)	σ (km s ⁻¹)	$\log M_{\text{BH}}$ ($\log M_{\odot}$)	$\log L_{\text{X}}$ [$\log(\text{erg s}^{-1})$]	$\log M_{\star}$ ($\log M_{\odot}$)
(1)	(2)	(3)	(4)	(5)	(6)	(7)	(8)	(9)
74	1488	I3487	16.50	15.03	28 ± 0	4.1	< 38.14	9.0
75	1779	I3612	16.50	14.97	...	6.7	< 38.14	9.0
76	1895	U7854	15.85	15.15	...	6.6	< 38.10	9.0
77	1499	I3492	16.50	15.15	...	6.7	38.42	8.8
78	1545	I3509	16.83	14.95	...	6.8	< 38.16	9.2
79	1192	N4467	16.50	14.74	83 ± 10	6.4	< 38.68	9.5
80	1857	I3647	16.50	15.06	...	6.7	< 38.14	9.0
81	1075	I3383	16.14	15.20	...	6.6	< 38.12	9.2
82	1948	...	16.50	15.76	...	6.4	< 38.14	8.8
83	1627	...	15.63	15.31	...	6.6	< 38.34	9.1
84	1440	I798	16.00	14.90	...	6.7	< 38.27	9.2
85	230	I3101	17.78	15.68	...	6.5	< 38.62	8.9
86	2050	I3779	15.78	15.37	...	6.5	< 38.10	9.0
87	1993	...	16.52	15.79	...	6.4	< 38.14	9.0
88	751	I3292	15.78	14.86	...	6.7	< 38.29	9.4
89	1828	I3635	16.83	15.29	...	6.6	< 38.16	9.1
90	538	N4309A	22.91	16.17	...	6.5	< 38.41	8.9
91	1407	I3461	16.75	15.25	...	6.6	< 38.35	9.1
92	1886	...	16.50	15.50	...	6.5	< 38.14	8.8
93	1199	...	16.50	16.00	...	6.3	< 38.14	9.0
94	1743	I3602	17.62	15.73	...	6.5	< 38.20	8.9
95	1539	...	16.90	15.36	...	6.6	< 38.16	8.9
96	1185	...	16.90	15.50	...	6.5	< 38.36	9.1
97	1826	I3633	16.22	15.78	...	6.4	< 38.12	8.8
98	1512	...	18.37	13.92	...	7.3	< 38.23	9.2
99	1489	I3490	16.50	16.10	...	6.3	< 38.14	8.7
100	1661	...	15.85	14.80	...	6.8	< 38.12	9.0

NOTE. — Col.: (1) ACSVCS target number (2) VCC source name; (3) Alternate name, from NCG or catalogs; (4) Distance (from surface brightness fluctuations method; Mei et al. 2007; see also Blakeslee et al. 2009). The average distance to the Virgo cluster – of 16.5 Mpc – is employed in case of no available distance modulus; (5) Extinction-corrected B magnitude, estimated as described in paper I; E(B-V) values are from Ferrarese et al. (2006b); (6) Stellar velocity dispersion, from ENEARc (Bernardi et al. 2002), unless otherwise indicated (for details, see caption of Table 2 in Paper I); (7) Black hole mass, estimated according to the ‘fiducial distribution’ described in § 4. of Paper I; (8) Nuclear luminosity between 0.3-10 keV, corrected for absorption; literature references are given in brackets; (9) Stellar mass of the host galaxy, in M_{\odot} , derived from g_0 and z_0 band AB model magnitudes following Bell et al. (2003), as described in Paper I.

TABLE 2
 GALAXIES HOSTING BOTH A NUCLEAR X-RAY SOURCE AND A MASSIVE NUCLEAR
 STAR CLUSTER.

ID	VCC	g (mag)	z (mag)	r_h ($''$)	$\log M_s$ (M_\odot)	$N(>L_X)$	$1 - P_X$ (%)
(1)	(2)	(3)	(4)	(5)	(6)	(7)	(8)
29	1619	17.15	15.61	0.324	8.1	0.42	34.29
30	1883	18.75	17.63	0.024	7.3	8.33	99.97
32	784	18.36	16.71	0.161	7.7	0.72	51.32
37	1250	19.75	18.22	0.026	7.2	8.59	99.98
47	1283	20.67	19.10	0.053	6.8	0.59	44.57
59	1355	21.11	20.10	0.043	6.3	0.11	10.42

NOTE. — Columns: (1) & (2) see Table 1; (3) & (4) g - and z - band magnitudes, from Ferrarese et al. (2006b); (5) & (6) half-light radius (from Ferrarese et al. 2006) and massive star cluster mass estimated following the prescription and mass-to-light ratio described in Ferrarese et al. (2006a); (7) Number of expected LMXBs with X-ray luminosity equal or greater than the measured X-ray core; (8) P_X is the chance probability that the *Chandra* PSF is contaminated by a LMXB of luminosity equal/higher than the measured one.

TABLE 3
X-RAY ACTIVE FRACTION & COMPLETENESS.

L_X/L_{Edd} (1)	# objects (2)	$10^{8.5-10.5} M_\odot$ (3)	$10^{10.5-12.0} M_\odot$ (4)
-9	4	0–100% (0/0)	25.1–98.8% (3/4)
-8	11	> 4.5% (1/1)	60.2–99.5% (9/10)
-7	13	19.3–80.6% (4/8)	> 48.3% (5/5)
-6	3	< 88.2% (0.41 ^a /2)	> 4.5% (1/1)

NOTE. — Columns: (1) Completeness limit in Eddington-scaled X-ray luminosity. (2) Total number of objects within the given completeness limit. (3) X-ray active fraction for host stellar masses ranging between $10^{8.5-10.5} M_\odot$. The number of active vs. total is given in parenthesis. (4) X-ray active fraction for host stellar masses ranging between $10^{10.5-12.0} M_\odot$. The number of active vs. total is given in parenthesis. *a*) Refers to the ‘weighted’ SMBH distribution (see § 3).